MULTIBODY DYNAMICS 2007, ECCOMAS Thematic Conference
C.L. Bottasso, P. Masarati, L. Trainelli (eds.)
Milano, Italy, 25–28 June 2007

# A MULTI-BODY DYNAMICS APPROACH FOR THE STUDY OF CRITICAL HANDLING MANOEUVRES ON SURFACES WITH UNEVEN FRICTION

**Manish Jaiswal[*], George Mavros [†], Homer Rahnejat[*] and Paul King[*]**

[*] Mechanical and Manufacturing Engineering
Loughborough University
Loughborough, Leicestershire LE11 3TU UK
e-mail: M.Jaiswal@lboro.ac.uk, H.Rahnejat@lboro.ac.uk, P.D.King@lboro.ac.uk

[†] Aeronautical and Automotive Engineering
Loughborough University
Loughborough, Leicestershire LE11 3TU UK
e-mail: G.Mavros@lboro.ac.uk

**Keywords:** Multi-body dynamics, simulation, handling, road friction, severe manoeuvres.

**Abstract.** *The study of the dynamic behaviour of vehicles using computer simulation has been one of the major areas of research for many years. Based on the application area, the models used for performing these studies vary greatly in their capability, complexity and amount of data required. The multi-body approach is most preferred when it comes to iterative design optimization, whereas relatively simple models are mostly used for studying basic handling characteristics and vehicle stability. However, for studies involving critical handling manoeuvres, it is imperative to include certain amount of detail in the vehicle model, which accounts for the influence of suspension geometry and tyre characteristics on handling behaviour.*

*The aim of the present research is to develop a vehicle model, based on Newton-Euler formulation of equations, incorporating sufficient degrees of freedom and adequate non linear characteristics for the realistic simulation of severe handling manoeuvres. The model is verified against experimental vehicle data and is finally used for the investigation of critical handling manoeuvres on surfaces with uneven friction. During this procedure, the tendency of the vehicle to rollover is assessed, together with other dynamic outputs such as yaw velocity and lateral acceleration*

## 1 INTRODUCTION

Computer simulation serves as a primary tool for the prediction, assessment and optimisation of vehicle handling behaviour. Central to every simulation attempt is a mathematical description of the handling dynamics of a vehicle. Such mathematical descriptions may vary in complexity from simple linear models with only few principal DOF (degrees-of-freedom) to more elaborate, non-linear multi-DOF models. Low-end linear models such as the so-called bicycle model are found in text books [1] and in many cases facilitate analytical solution of the equations of motion. While the predictions by such models lack accuracy, the results reveal the fundamentals of the theory of vehicle handling, as demonstrated in [1].

At the opposite end, complex multi-body-dynamics vehicle models [2-5], [6] account for the effects of flexible couplings between vehicle sub-components, geometrical and other non-linearities, as well as various kinematic constraints. The underlying theory required for modelling such elaborate dynamic systems is presented in text-books [7], [8] and is primarily based on the application of the constrained Lagrange equation [7],[8]. In general, the modelling process involves the assignment of a frame of reference and six DOF to each rigid-body component of the vehicle. The influence of mechanical joints and couplings is modelled mathematically by linking various DOF of different bodies using holonomic / non-holonomic constraints. The reaction forces within the constraints are calculated as the Lagrange multipliers [7], [8] by solving simultaneously the combined differential/algebraic system of equations, which results from the consideration of the constrained Lagrange equations for all possible degrees-of-freedom within the system. A detailed account of various multi-body approaches in vehicle dynamics and associated software packages is provided in [9].

A third modelling approach lies in-between the two aforementioned extremes. Using the Newton-Euler formulation for the derivation of the equations of motion, it is possible to derive non-linear multi-body models for the simulation of handling dynamics [10]. This approach can provide sufficiently accurate results for use in prediction, assessment and optimisation studies. Moreover, it requires less computational effort than any method based on the constrained Lagrange equation. This combination of qualities has made this approach a keen alternative in control studies [11]. However, the quality of models obtained by the Newton-Euler approach is susceptible to inaccuracies induced by various assumptions/simplifications made during the derivation process. When the aim is the study of severe handling manoeuvres with direct implications for passenger safety, accuracy holds a greater importance than computational efficiency.

The aim of the present research is to develop an intermediate multi-body model for the study of critical manoeuvres. In an attempt to keep computational effort to a minimum, the Newton-Euler approach is chosen. At this point, an additional advantage of such intermediate models should be emphasized. The relatively simple structure of these models allows general trends to be observed in relation to vehicle parameters. This leads to useful conclusions which might be significantly more difficult to draw when working with more complex models which exhibit a large number of interactions. As a result, researchers often rely on simple models when it comes to parametric investigation, avoiding the use of high-end multi-body software packages [12], [13], [14]. To enhance the accuracy of the proposed vehicle model, special attention is paid to the inclusion of suspension effects in a realistic manner. This involves the modelling of all suspension components, such as springs, dampers and anti-roll bars, as well as calculating rigid suspension reactions using the virtual work method [15, 16].

In addition, the brake system is modelled mathematically, for the ability of realistic simulation of braking manoeuvres in the future. The proposed vehicle model is validated against a detailed multi-body model developed in ADAMS multi-body software. At a second stage, it is demonstrated that the results obtained by the model agree to a rather satisfactory level with detailed experimental measurements. Finally, having gained confidence in the accuracy of the model, a number of critical handling manoeuvres are simulated, in particular related to cornering on surfaces with uneven friction. The propensity to roll-over is assessed, as the tyres suddenly enter areas of significantly higher friction during cornering.

## 2 MATHEMATICAL MODELLING

### 2.1 Motion Equations for the Vehicle Body

The primary dynamics of the vehicle relate to the six motions of the sprung mass in space. These are observed with respect to the moving SAE frame of reference [17], which is attached to the sprung part of the vehicle body, following its three displacements and three rotations in space. This choice agrees with common practice [10] and relates to the fact that most external forces such as tyre and aerodynamic forces are more easily expressed in the vehicle local frame of reference, than in the global frame. Also, results are more informative when presented as vehicle-based velocities/displacements, than when using the global frame of reference.

The complete vehicle model including the sprung mass and four un-sprung masses consisting of the wheels, tyres and part of the suspension, is shown in figure 1. While the sprung-mass is allowed a complete six DOF motion in space, the un-sprung masses move only in the vertical direction, with an additional rotational DOF to capture the rotation of the wheels about their spin axes. This approach leads to a vehicle model with a total of 14 DOF.

The equations of motion of the sprung mass are derived according to [10], and are expressed with respect to the vehicle SAE frame of reference, also shown in figure 1. The vehicle is assumed geometrically symmetrical about the X-Z plane of the SAE frame. However, the general case is considered, in which the vehicle is not inertially symmetrical about the same plane, i.e. the various products of inertia need not equal zero. The only restriction adopted is that the origin of the SAE frame lies at the same longitudinal position as the cg (centre of gravity). This requirement has no mathematical significance and is considered only to achieve general comparability of the results with the implications of analytical results obtained by simple bicycle models, where the origin of the SAE frame is usually taken at the position of the cg [1]. Considering the above, the equations of motion for the three translational and three rotational DOF, are given below:

$$\Sigma F_x = m_T \cdot \left(dU/dt - V \cdot r + W \cdot q\right) - m_T \cdot \left[x_G \cdot \left(q^2 + r^2\right) - y_G \cdot \left(p \cdot q - dr/dt\right) - z_G \cdot \left(p \cdot r + dq/dt\right)\right] \quad (1)$$

$$\Sigma F_y = m_T \cdot \left(dV/dt - W \cdot p + U \cdot r\right) - m_T \cdot \left[y_G \cdot \left(r^2 + p^2\right) - z_G \cdot \left(q \cdot r - dp/dt\right) - x_G \cdot \left(p \cdot q + dr/dt\right)\right] \quad (2)$$

$$\Sigma F_z = m_s \cdot \left(dW/dt - U \cdot q + V \cdot p\right) - m_S \cdot \left[z_G \cdot \left(p^2 + q^2\right) - x_G \cdot \left(p \cdot r - dq/dt\right) - y_G \cdot \left(q \cdot r + dp/dt\right)\right] \quad (3)$$

$$\Sigma M_x = I_{xx}\cdot\left(dp/dt\right)-\left(I_{yy}-I_{zz}\right)\cdot q\cdot r+I_{yz}\cdot\left(r^2-q^2\right)-I_{zx}\cdot\left(p\cdot q+dr/dt\right)$$
$$+I_{xy}\cdot\left(p\cdot r-dq/dt\right)+m_S\cdot y_G\cdot\left(dW/dt-U\cdot q+V\cdot p\right)-m_S\cdot z_G\cdot\left(dV/dt-W\cdot p+U\cdot r\right) \quad (4)$$

$$\Sigma M_y = I_{yy}\cdot\left(dq/dt\right)-\left(I_{zz}-I_{xx}\right)\cdot p\cdot r+I_{xz}\cdot\left(p^2-r^2\right)-I_{xy}\cdot\left(q\cdot r+dp/dt\right)$$
$$+I_{yz}\cdot\left(q\cdot p-dr/dt\right)+m_S\cdot z_G\cdot\left(dU/dt-V\cdot r+W\cdot q\right)-m_S\cdot x_G\cdot\left(dW/dt-U\cdot q+V\cdot p\right) \quad (5)$$

$$\Sigma M_z = I_{zz}\cdot\left(dr/dt\right)-\left(I_{xx}-I_{yy}\right)\cdot p\cdot q+I_{xy}\cdot\left(q^2-p^2\right)-I_{yz}\cdot\left(r\cdot p+dq/dt\right)$$
$$+I_{zx}\cdot\left(r\cdot q-dp/dt\right)+m_T\cdot x_G\cdot\left(dV/dt-W\cdot p+U\cdot r\right)-m_T\cdot y_G\cdot\left(dU/dt-V\cdot r+W\cdot q\right) \quad (6)$$

In the above equations $U$, $V$, $W$, denote the three translational velocities of the sprung mass along the X, Y and Z axes of the SAE frame respectively, while $p$, $q$, $r$ are the rotational speeds (roll, pitch, yaw) about the same axes. The left-hand-side terms in eq. (1)-(6) denote the net forces in the direction of the X, Y and Z axes, or the net moments about the same axes. In terms of inertial properties, $m_T$ denotes the total mass of the vehicle, including the mass of the un-sprung components. It is interesting to note that $m_T$ appears only in eq. (1), (2), as the longitudinal and lateral DOF are subject to the vehicle's total inertia. On the contrary, when dealing with the vertical motion, it is more appropriate to use the sprung mass, $m_S$. Similar comments apply for the use of $m_S$ in eq. (4), (5) and $m_T$ in eq. (6). An alternative – and mathematically sounder – approach would be to use the sprung mass $m_S$ throughout eq. (1)-(6) and provide all un-sprung masses with additional lateral and longitudinal degrees-of-freedom. This would bring the model closer to its complex multi-body alternatives, increasing unnecessarily the computational cost of the simulation. It is important to emphasize that the treatment of mass presented herein is a simplification which aims to distribute the mass more appropriately between various degrees-of-freedom, without increasing their number and without introducing additional constraints. In the same spirit, parameters $x_G$, $y_G$, $z_G$ indicate the distance of the cg of the complete vehicle from the origin of the SAE frame of reference. According to the restriction described earlier regarding the longitudinal position of the cg, the following relation applies:

$$x_G = 0 \quad (7)$$

Finally, $I_{xx}, I_{yy}$ indicate the sprung mass moments of inertia about the X and Y axes, whereas $I_{zz}$ denotes the moment of inertia of the full vehicle about the Z axis. The products of inertia $I_{xy}$, $I_{zx}$ and $I_{yz}$ are all calculated considering the un-sprung mass only.

The forces on the left-hand-side of eq. (1)-(3) include those developed at the tyre contact patch, due to gravity, suspension reactions, as well as aerodynamic forces. In many cases, the roll and pitch angles of the vehicle body (denoted $\phi$ and $\theta$, respectively) can be assumed small enough so that the X-Y plane of the SAE frame is considered always parallel to a flat road. Under these circumstances the calculation of forces $\Sigma F_x$, $\Sigma F_y$ and $\Sigma F_z$ is a rather straight forward procedure. However, under extreme cornering and/or braking manoeuvres, large roll and pitch angles require the determination of the exact position of the SAE frame

with respect to the global frame of reference. In this way, a tyre force which is parallel to the road is not assumed parallel to the X-Y plane, or, conversely, a vertical suspension force is not assumed parallel to the Z-axis of the SAE frame. To solve the problem, all forces on the left-hand-side of eq. (1)-(3) are multiplied by a transformation matrix resulting from three successive rotations $\psi$, $\theta$, $\phi$, (yaw, pitch, roll) as shown below [18]:

$$L(\psi,\theta,\phi)=\begin{bmatrix} \cos\theta\cos\psi & \cos\theta\sin\psi & -\sin\theta \\ \sin\phi\sin\theta\cos\psi-\cos\phi\sin\psi & \cos\psi\cdot\cos\phi+\sin\phi\sin\theta\sin\psi & \sin\phi\cos\theta \\ \cos\phi\sin\theta\cos\psi+\sin\phi\sin\psi & \cos\phi\sin\theta\sin\psi-\sin\phi\cos\psi & \cos\phi\cdot\cos\theta \end{bmatrix} \tag{8}$$

Due to the fact that the angles of rotation cannot be assumed small, angles $\psi$, $\theta$, $\phi$ are not calculated by direct integration of rotational velocities $r$, $q$, $p$. Instead, an angular velocity transformation is required, similar to the transformations used frequently in aircraft dynamic analysis [18]. Such transformations relate the instantaneous rotational velocities as expressed in the vehicle frame of reference, to angular rates as expressed in the global frame of reference. Provided that $r$, $q$, $p$ are calculated by solving the differential equations (4)-(6), the following transformation provides the corresponding rates in the global frame [18]:

$$\begin{bmatrix} \dot{\phi} \\ \dot{\theta} \\ \dot{\psi} \end{bmatrix}=\begin{bmatrix} 1 & \sin\phi\tan\theta & \cos\phi\tan\theta \\ 0 & \cos\phi & -\sin\phi \\ 0 & \sin\phi/\cos\theta & \cos\phi/\cos\theta \end{bmatrix}\begin{bmatrix} p \\ q \\ r \end{bmatrix} \tag{9}$$

Finally, integration of eq. (9) yields the corresponding angles for use in the transformation matrix described by relation (8). Accordingly, the sums of moments on the left-hand-side of eqs. (4)-(6) are calculated based on the forces expressed in the SAE frame of reference, i.e. following transformation.

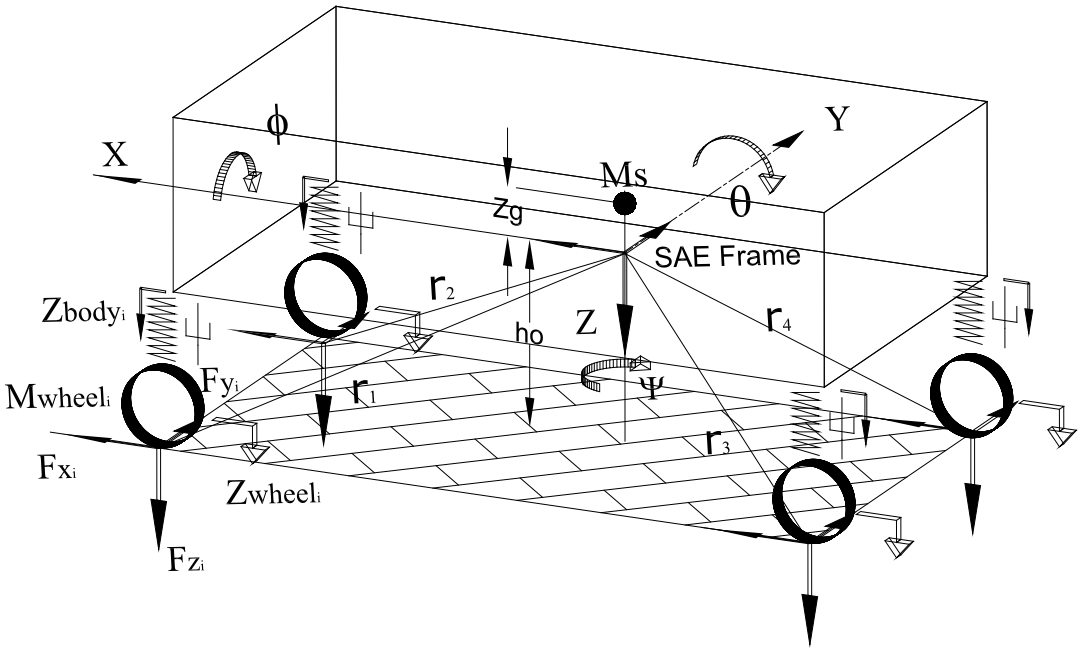


**Figure 1 Vehicle Model including the SAE frame of reference**

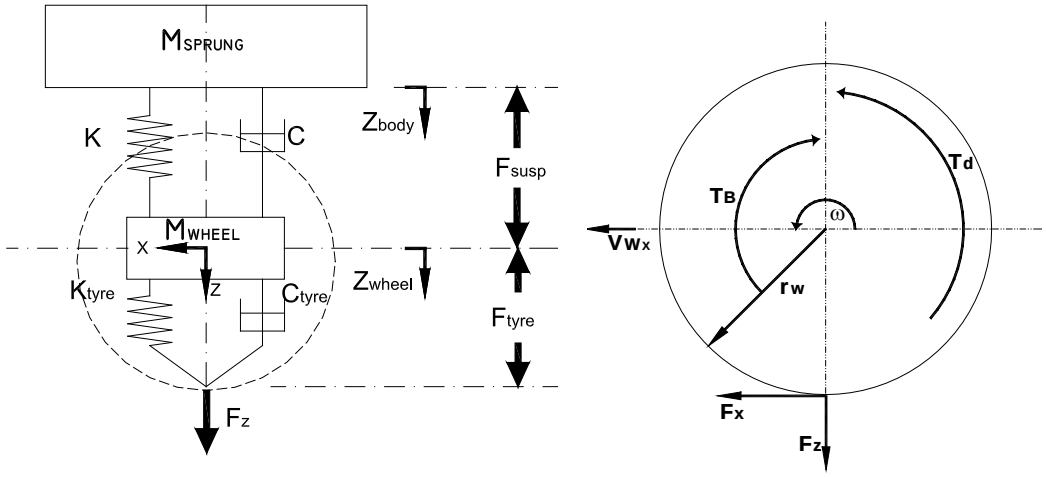


**Figure 2 Suspension and Wheel Free Body Diagram**

## 2.2 Suspension and Wheel Dynamics

In terms of vertical dynamics, the wheels, including part of the suspension mass are modelled as single DOF mass-spring-damper systems. The tyres are considered as linear spring-damper systems which connect the un-sprung masses to the road. At the top end, the un-sprung masses are connected to the vehicle body using springs and dampers representing non-linear wheel-rates and damping functions. Non-linearities result from the geometry of the suspension and are treated using the suspension-ratio concept [19] and also from the consideration of different bump/rebound damper settings. A schematic of the suspension model is provided in fig. 2. The spring-damper forces due to the relative motion of the un-sprung masses with respect to the body are given below:

$$F_{susp_1} = -K_f[\underbrace{\left(z - t_{rf}\cdot\phi - a\cdot\theta\right)}_{z_{body_1}} - z_{wheel_1}] - C_f[\underbrace{\left(\dot{z} - t_{rf}\cdot p - a\cdot q\right)}_{\dot{z}_{body_1}} - \dot{z}_{wheel_1}] \tag{10}$$

$$F_{susp_2} = -K_f[\left(z + t_{rf}\cdot\phi - a\cdot\theta\right) - z_{wheel_2}] - C_f[\left(\dot{z} + t_{rf}\cdot p - a\cdot q\right) - \dot{z}_{wheel_2}] \tag{11}$$

$$F_{susp_3} = -K_r[\left(z - t_{rr}\cdot\phi + b\cdot\theta\right) - z_{wheel_3}] - C_r[\left(\dot{z} - t_{rr}\cdot p + b\cdot q\right) - \dot{z}_{wheel_3}] \tag{12}$$

$$F_{susp_4} = -K_r[\left(z + t_{rr}\cdot\phi - b\cdot\theta\right) - z_{wheel_4}] - C_r[\left(\dot{z} + t_{rr}\cdot p - b\cdot q\right) - \dot{z}_{wheel_4}] \tag{13}$$

In the above equations, $p$ and $q$ are the roll and pitch rates of the vehicle body, $z$ is the vertical displacement of the vehicle body, $\phi$ and $\theta$ are the roll and pitch angles as calculated by integration of eq. (9) and $z_{wheel_{1-4}}$ denotes the vertical displacements of the four wheels. $K_{f,r}$, $C_{f,r}$ indicate non-linear wheel-rate and damping functions. Finally, $a$, $b$ denote the distance of the origin of the SAE frame from the front and rear axles respectively and $t_{rf}$, $t_{rr}$ are the front and rear half-tracks. Considering the expressions for the suspension forces and further

including the effect of the anti-roll bars and rigid suspension reactions, the equations for the vertical motion of the un-sprung masses are derived as follows:

$$-F_{susp_1}-\underbrace{\left[K_{tyre}z_{wheel_1}+C_{tyre}\dot{z}_{wheel_1}\right]}_{F_{tyre_1}}+M_{wheel_1}\cdot g\ -\ M_{wheel_1}\cdot\ddot{z}_{wheel_1}-\underbrace{\frac{K_{roll}(\phi+\phi_{wheel_1})}{2\cdot t_{rf}}}_{F_{antiroll_1}}-F_{zy_1}-F_{zx_1}=0 \qquad (14)$$

$$-F_{susp_2}-K_{tyre}z_{wheel_2}-C_{tyre}\dot{z}_{wheel_2}+M_{wheel_2}\cdot g\ -\ M_{wheel_2}\cdot\ddot{z}_{wheel_2}+\frac{K_{roll}(\phi+\phi_{wheel_2})}{2\cdot t_{rf}}-F_{zy_2}-F_{zx_2}=0 \qquad (15)$$

$$-F_{susp_3}-K_{tyre}z_{wheel_3}-C_{tyre}\dot{z}_{wheel_3}+M_{wheel_3}\cdot g\ -\ M_{wheel_3}\cdot\ddot{z}_{wheel_3}-\frac{K_{roll}(\phi+\phi_{wheel_3})}{2\cdot t_{rr}}-F_{zy_3}-F_{zx_3}=0 \qquad (16)$$

$$-F_{susp_4}-K_{tyre}z_{wheel_4}-C_{tyre}\dot{z}_{wheel_4}+M_{wheel_4}\cdot g\ -\ M_{wheel_4}\cdot\ddot{z}_{wheel_4}+\frac{K_{roll}(\phi+\phi_{wheel_4})}{2\cdot t_{rr}}-F_{zy_4}-F_{zx_4}=0 \qquad (17)$$

For the calculation of the forces due to the anti-roll bars in eq. (14)-(17), an additional equivalent roll-angle $\phi_{wheel_{1-4}}$ is employed, in order to account for force generation due to unequal left and right vertical wheel displacement. Such conditions occur in the event of the vehicle running on undulated roads. The additional equivalent roll angle, $\phi_{wheel_{1-4}}$, is calculated based on simple geometrical considerations as shown in eq. (18)-(19), and is subsequently added to the actual vehicle body roll angle, $\phi$. Finally, $F_{zx}$, $F_{zy}$ are the rigid suspension reactions which are calculated using the virtual work method, as explained in detail in the next section.

$$\phi_{wheelf}=\text{atan}\frac{z_{wheel1}-z_{wheel2}}{2\cdot t_{rf}} \qquad (18)$$

$$\phi_{wheelr}=\text{atan}\frac{z_{wheel3}-z_{wheel4}}{2\cdot t_{rr}} \qquad (19)$$

The rotational dynamics of all wheels are included in the study, to facilitate simulation of the variation of longitudinal slip angle under braking manoeuvres. In addition, a simple PID controller is implemented in order to be able to maintain constant forward speed under various manoeuvres and ultimately achieve comparability with constant speed experimental results. The controller regulates the diving torque at the driving wheels using as feedback error the difference between target and actual forward speed.

Referring to fig. 2 the rotational motion of a driven wheel is described by equation (20), taking into account the driving/braking torques and the longitudinal force generated by the tyre.

$$\dot{\omega}=\frac{T_d-F_x\cdot r_w-T_b}{I_{wheel}} \qquad (20)$$

### 2.3 Suspension Rigid Reactions

The vertical motion of the centre of the tyre contact patch is associated with secondary lateral and longitudinal motions, as a result of the complex suspension geometries used in practice. Hence, an infinitesimal vertical displacement $\partial z_{contact}$ is almost always coupled with displacements $\partial x_{contact}$ and $\partial y_{contact}$. This observation allows treatment of the suspension as a kinematic mechanism where the kinematic input point is chosen as the centre of the tyre contact patch, with two possible input-motion directions, i.e. lateral and longitudinal. The output is taken as the vertical motion of the tyre contact centre with respect to the vehicle body. If the lateral, $F_y$, and longitudinal, $F_x$, forces at the centre of the contact patch are known, application of the virtual work method [15, 16] yields the resulting vertical forces applied on the sprung mass, as described in relations (21) and (22).

$$F_{zy} = -F_y \frac{\partial y_{contact}}{\partial z_{contact}} \tag{21}$$

$$F_{zx} = -F_x \frac{\partial x_{contact}}{\partial z_{contact}} \tag{22}$$

It should be emphasized that eq. (21), (22) hold true for all four corners of the vehicle as long as the vehicle-based SAE frame of reference is used both for the expression of the displacements and forces.

Equations (21) and (22) account for all jacking, anti-dive, anti-roll and related phenomena, offering an alternative to the frequently used roll-centre concept [20] and other similar treatments. The application of the virtual work method requires only the establishment of the lateral and longitudinal displacements as functions of the vertical displacement of the contact centre. Subsequently, it allows the non-linear treatment of rigid suspension reactions, avoiding complications related to phenomena such as roll-centre migration.

### 2.4 Tyre Model

Tyre forces are calculated based on the version of the Magic Formula tyre model presented in [21]. The general form of the formula reads:

$$y = D\sin\left[C\arctan\left\{Bx - E\left(Bx - \arctan Bx\right)\right\}\right] \tag{23}$$

$$Y(X) = y(x) + S_V \tag{24}$$

$$x = X + S_H \tag{25}$$

Where $X$ represents the primary input variable (in the form of side-slip or longitudinal slip) and $Y$ represents the primary output variable (in the form of lateral/longitudinal force or self-aligning torque).

The primary parameters of the Magic formula, namely $B, C, D, E, S_H$ and $S_V$, appear as functions of the normal load, $F_z$, the camber angle, $\gamma$, and a number of secondary constants [9].

Tyre shear forces as generated by the Magic Formula are expressed in the tyre SAE frame of reference [17]. When a wheel is running steered on a flat road, the actual tyre forces, $F_{xtyre}$, $F_{ytyre}$ require a single transformation based on the steer-angle, $\delta$, in order to be expressed in the vehicle SAE frame of reference. This is shown in eq. (26), (27). Obviously, in the case of large roll and pitch angles, the forces, $F_x$, $F_y$ calculated by these equations require further transformation using relation (8).

$$F_x = \left(F_{xtyre}\right) \cdot \cos\delta - \left(F_{ytyre}\right) \cdot \sin\delta \tag{26}$$

$$F_y = \left(F_{xtyre}\right) \cdot \sin\delta + \left(F_{ytyre}\right) \cdot \cos\delta \tag{27}$$

## 2.5 Brake System

The brake system incorporated in the vehicle model is adopted from a previous study carried out in [22]. Instead of a detailed representation of the complete brake system as done by [23] and [24], a reduced order model of the brake system dynamics is used, which considers simplified brake hydraulics and a vacuum booster. The model is suited for further extension to ABS control. The vacuum booster is divided into two chambers: the vacuum chamber is connected to the engine manifold, whereas the apply chamber is either connected to the atmospheric pressure, the vacuum chamber, or stays sealed, depending upon the valve settings. The vacuum booster provides a simple yet robust amplification to the brake pedal force, by exploiting the pressure difference, between the atmosphere and engine intake manifold. In doing so, it undergoes three stages of operation: the release stage, the apply stage and the hold stage. The operation of these stages is modelled by taking into consideration the static force balance and air flow dynamics, including effects such as vacuum booster hysteresis, which occurs due to reaction washer deformation and master cylinder seal friction. The mechanical control valve modulates the air flow in the vacuum booster, based on the force response from the brake pedal, and thus provides a feedback mechanism to set the three stages of booster operation.

The air flow dynamics in the vacuum booster are modelled assuming ideal gas behaviour and isothermal expansion. The assumption of an incompressible flow is valid as it simplifies the system for use in control studies, yet does not affect the results dramatically [22]. When considering the brake system hydraulics, the state variable is represented in terms of the volume of fluid displaced into each wheel cylinder. The brake hydraulics itself could be divided into two circuits, which are connected to a tandem master cylinder containing two pistons arranged in a single bore. Thus the primary and secondary master cylinder circuits are connected to two wheel cylinders each, preferably using the diagonal split, connecting a front and a rear wheel.

## 3 MULTI-BODY MODEL IN ADAMS/CHASSIS

To facilitate the comparative study with the intermediate, lumped mass model, a detailed multi-body vehicle model was developed in the ADAMS/Chassis environment. ADAMS/Chassis is one of the modules offered in ADAMS software dedicated to vehicle dynamic analysis. ADAMS/Chassis module offers a comprehensive library of vehicle components and subsystems. One of the advantages in using ADAMS/Chassis is that it enables simulation of full-vehicle dynamic events such as steady-state drift, double lane change, constant radius etc. as well as half-vehicle events such as dynamic load case etc. These events are readily available within an extensive list of ride, handling and durability events. Figure 3 shows a graphical representation of the vehicle model built in the ADAMS/Chassis environment.

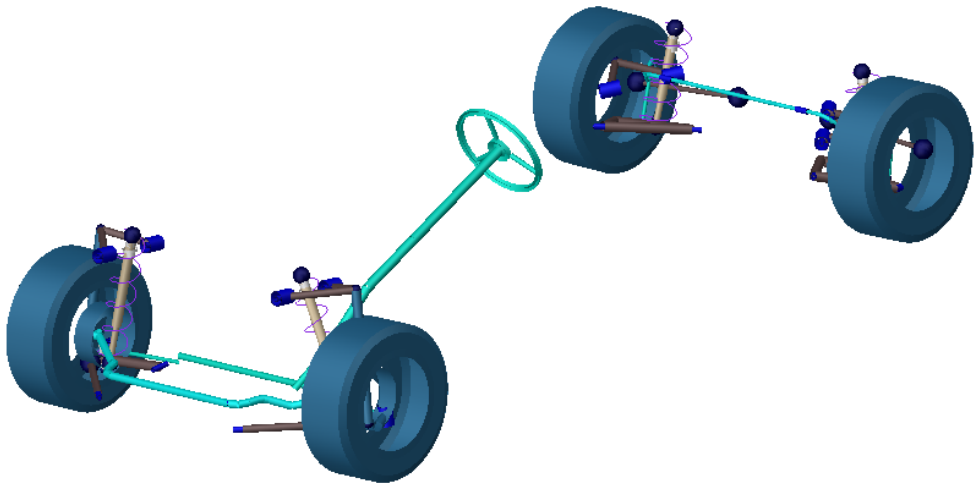

**Figure 3 Multi-Body Model of Passenger Car in ADAMS Chassis**

## 4 VEHICLE HANDLING ANALYSIS

In the present work, three individual handling studies are conducted. First, the intermediate, 14 DOF multi-body model is compared with its complex multi-body counterpart developed in ADAMS/Chassis. Subsequently, the 14 DOF model is subjected to real-life manoeuvres and the results are compared with experimental measurements. Finally, the model is used in order to carry out a virtual study of severe handling manoeuvres involving cornering on surfaces with uneven friction.

### 4.1 Comparison Between 14 DOF and ADAMS Models

Comparison of the two vehicle models is performed on the basis of two separate manoeuvres, namely a J-turn and a double-lane change manoeuvre.

The J-turn test is a single-steer manoeuvre test used to study the transient handling properties of a vehicle at limiting cornering conditions. The test is conducted by driving at a constant speed and applying a pre-set steering input of 90 degrees at the steering wheel. The steering input approximates a steep ramp increase in steering-wheel angle at a rate of $512^{o}$/s. This manoeuvre assesses the vehicle's open loop response to an almost step input and is often used to evaluate vehicle properties, particularly in relation to roll stability. In the current J-

Turn simulation, the vehicle velocity is set to 70 Km/h and a steering-wheel angle of -90 degree was applied for a left hand turn, as shown in the first graph of Figure 4.

The lateral acceleration, yaw rate, roll angle, and resulting path as predicted by the two models are illustrated in Figure 5. The first observation to be made is that results obtained by the two models correlate well. Probably the most informative graph is that showing the yaw rate response with time. It can be seen that, compared to the 14 DOF model, the ADAMS model exhibits a rather oscillatory yaw rate response with a larger overshoot. This behaviour points towards additional under-steer which almost certainly can be attributed to the additional suspension and steer compliance incorporated in the more detailed multi-body model. At this point it should be noted that the weight distribution of the actual vehicle is such that an inherently under-steering behaviour is expected. This behaviour, however, is emphasized by the additional compliance built into the ADAMS model.

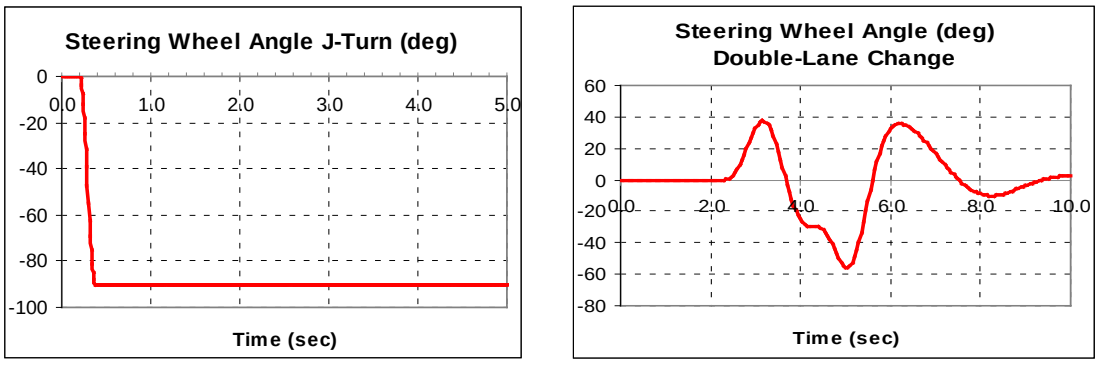


**Figure 4 Steering Wheel Angle for J-Turn and Double-Lane Change**

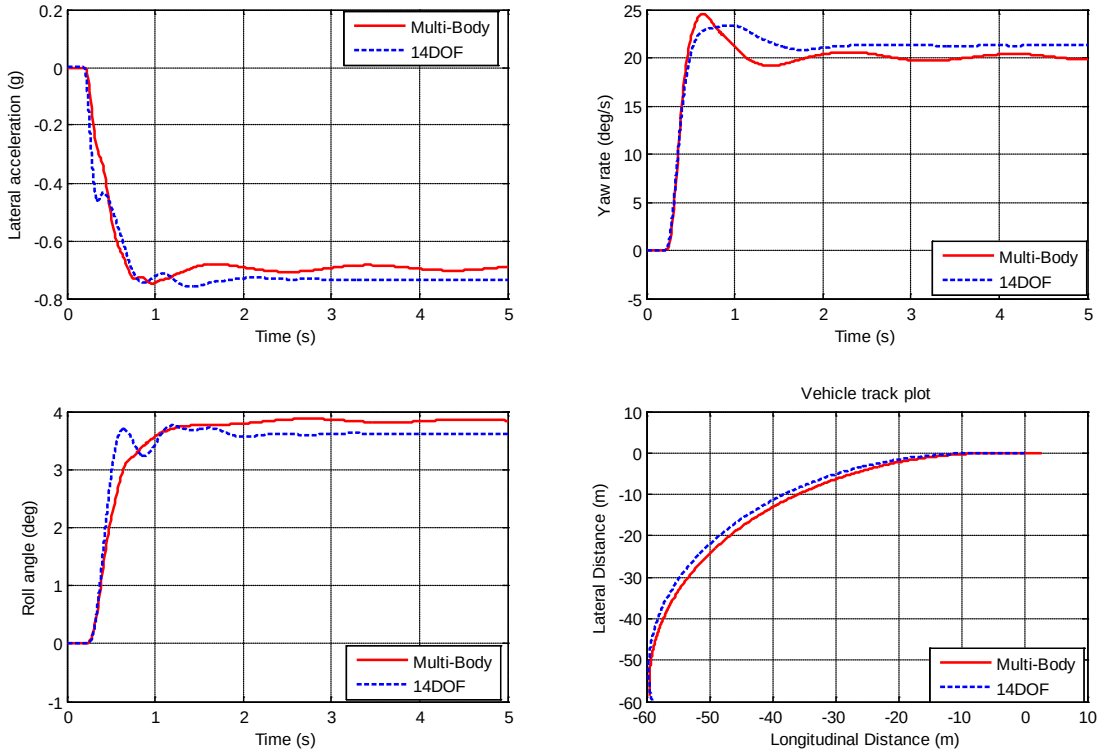


**Figure 5 Vehicle Handling Responses for J-Turn**

The second comparative test involves a double-lane-change manoeuvre. The double-lane-change manoeuvre is an inherently subjective test standardised by ISO [25]. The subjective character of the specific test is related to its closed-loop nature. The test-driver is required to drive at a pre-specified speed through a path precisely marked by traffic cones. The path resembles that of a vehicle performing a rather tight overtaking manoeuvre, while the driver is free to correct the steer-angle according to his/her will. Although the primary aim of the test is usually the subjective assessment of the responsiveness of the vehicle, in the present study the test is carried out in an open-loop fashion, with a prescribed steering input as shown in the second graph of figure 4. Simulations were performed at a forward speed of 100 kph and the lateral acceleration, yaw rate, roll angle, and vehicle path are shown in Figure 6. Again, good correlation is observed between the two models with only small differences evident.

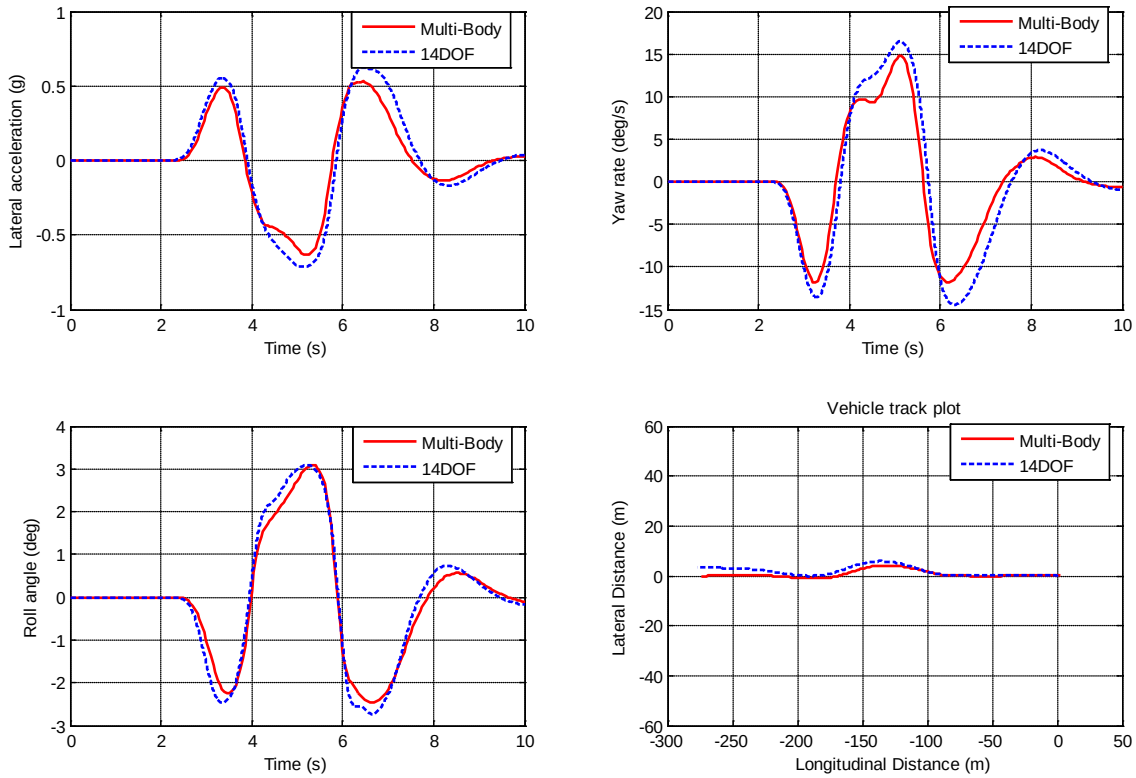


**Figure 6 Vehicle Handling Responses for Double-Lane Change**

## 4.2 Experimental Validation of the 14 DOF model

To further test the accuracy of the intermediate model, a series of experimental measurements were carried out on the actual vehicle which formed the basis for the computer models. The vehicle was equipped with an RT3200 GPS/Inertial measurement system which provided all six vehicle states, while the steer-angle and other information such as rotational wheel speeds were obtained from the vehicle's CAN network. Testing was carried out on a flat proving ground and the vehicle was – in most cases – forced to operate in its non-linear region where the accuracy of simplified models usually deteriorates. In the present paper, only two out of a significant number of tests are presented.

During the first test, the vehicle was subjected to an arbitrary steering input, as shown in the first graph of figure 7. The forward speed was maintained at approximately 50 kph, which, given the magnitude of the steering, proved sufficient for the achievement of medium to high values of lateral acceleration. As demonstrated in figure 7, the results obtained by the 14 DOF model show good agreement with experimental results in terms of lateral acceleration, yaw rate and roll angle. The small discrepancies between the two models do not allow direct conclusions to be made as to what are the sources of the observed differences.

Additional ground for comments is offered by the second experimental test, involving a severe step-steer manoeuvre at a forward speed of approximately 50 kph. The steering-input together with experimental and simulation results for this test are given in figure 8. Good correlation between experimental and simulation results is still evident, while the experimental yaw rate response shows a longer rise-time, which points towards a slightly more over-steering behaviour. Assuming that the main difference between the real vehicle and the model relates to the existence or not of suspension and steering compliances, the behaviour of the real vehicle would be expected to shift towards under-steer. This effect has already been discussed in the comparison between the 14 DOF and the ADAMS model in the preceding section. Observing the opposite effect could be attributed to differences between the real tyres and the nominal tyre model used in the simulation. Such differences might be further intensified by arbitrarily changing road-tyre friction conditions. For example, during testing, a number of relatively wet patches were observed on the proving ground.

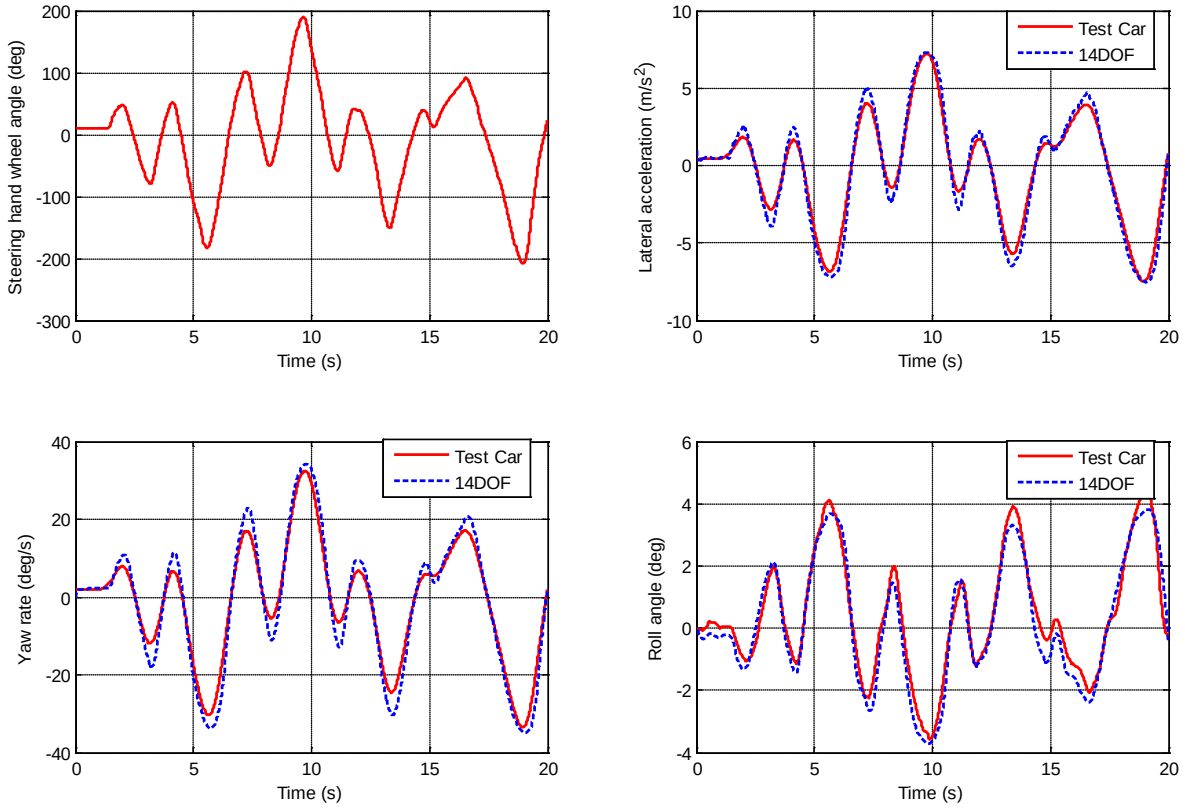


**Figure 7 Vehicle Handling Responses to an Arbitrary Steer-Input**

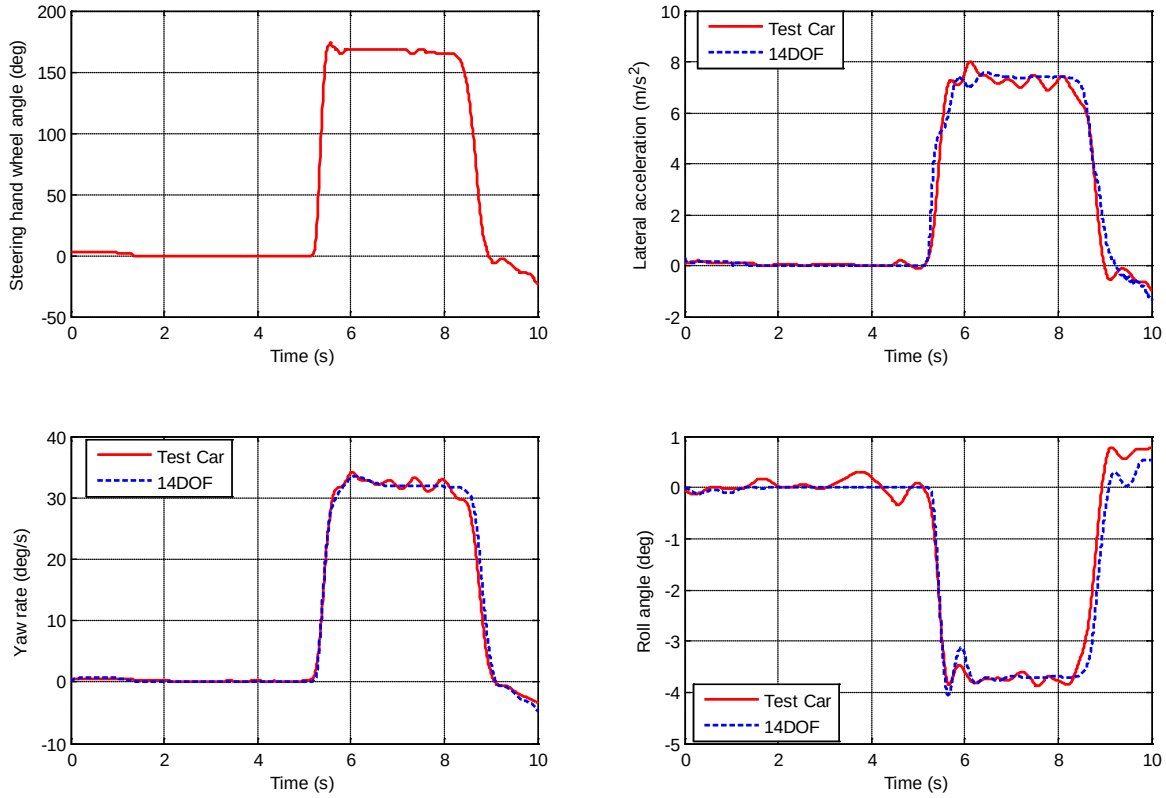


**Figure 8 Vehicle Handling Responses to Step-Steer Input**

### 4.3 Transient Manoeuvre on a Surface with Uneven Friction

Thus far the model has been tested under conditions which promote operation in the non-linear area. In all cases, good agreement was observed between the results generated by the intermediate model and those obtained the real vehicle, or the more elaborate multi-body model. The success of the intermediate model can be attributed mainly to the careful consideration of the influence of suspension mechanics in vehicle handling dynamics. A realistic representation of the suspension and a modelling approach appropriate for the treatment of large roll angles is critical for the simulation of severe manoeuvres which are likely to lead to vehicle roll-over. Although the vehicle under consideration is inherently stable with respect to roll (due to large front and rear tracks), a couple of simulation studies were conducted to explore its handling behaviour at the limit.

The first test involves a step-steer input of more than $100^{o}$ at an initial forward speed of 120 kph. Road-tyre friction is assumed even and the peak factor, $D$, of the Magic Formula is modified to generate a peak force corresponding to a coefficient of friction $\mu = 1$ under static corner load. It is important to note that during this test the forward speed is allowed to reduce as a result of the steering input, i.e. the forward speed PID controller is deactivated. The yaw-rate response depicted in figure 9 indicates under-steering behaviour, while the tyre vertical loads show clearly that all four tyres remain in contact with the ground.

The second test case involves an identical steer input performed at the same initial speed of 120 kph. The coefficient of road-tyre friction starts at a value of $\mu = 0.5$, however, during

the manoeuvre, the two outer tyres suddenly enter a part of the road where friction is significantly higher, attaining a value of $\mu = 2.5$. Although this value of friction appears rather unrealistic for a passenger vehicle running on a normal road, it can be used as a means of simulating the situation where tyre side-forces increase abruptly as a result of the wheels meeting with an obstacle, such as the edge of a low pavement. The first thing that becomes apparent by observing figure 10, is a discontinuity which appears more distinctly in the lateral acceleration, yaw rate and roll rate responses. This discontinuity coincides with the moment in time when the two outer tyres enter the part of the road with increased friction. Although the manoeuvre starts with a lower lateral acceleration due to reduced road friction, the subsequent increase in friction is sufficient to cause lift-off for both inner wheels after approximately 1.5 seconds. It is interesting to note that in terms of its yaw rate response the vehicle remains stable, persisting on its under-steering qualities. Finally, the inherently stable character of the vehicle in terms of its roll motion is highlighted by the modest roll angle, even at high lateral accelerations (above 1.5g)

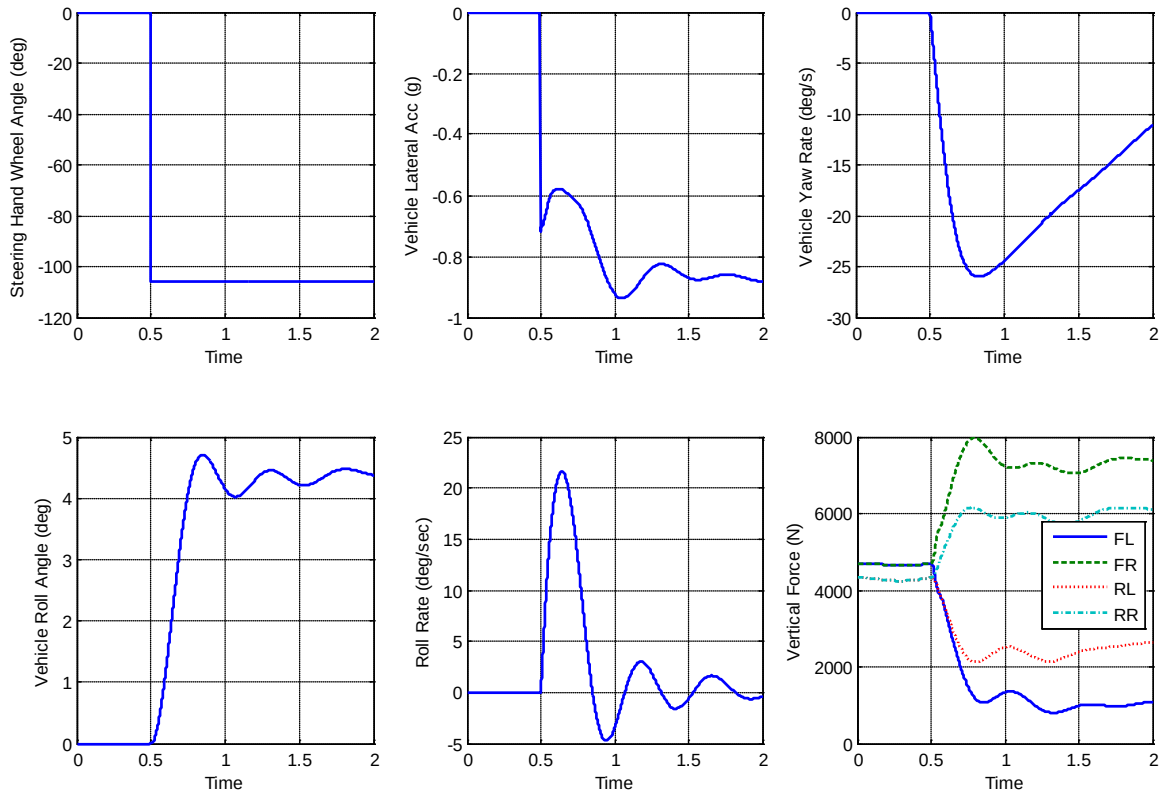


**Figure 9 Responses to a Step-Steer Manoeuvre on a Surface with Even Friction**

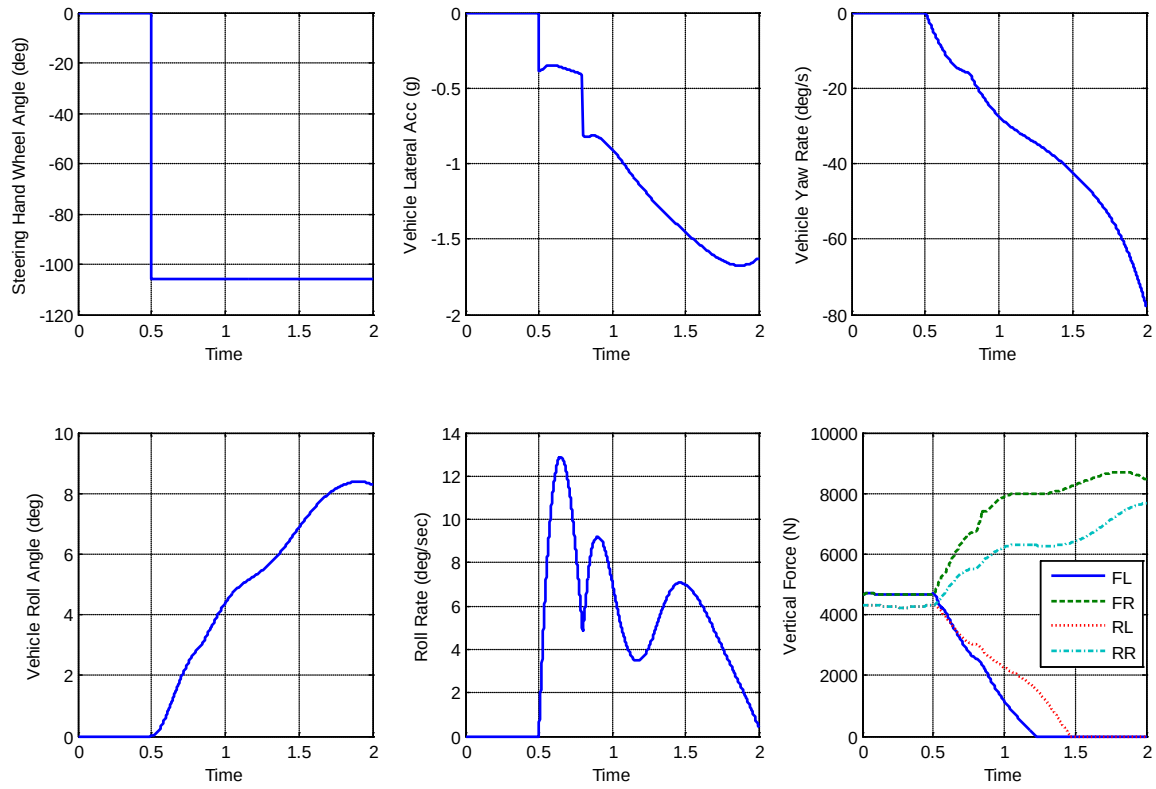


**Figure 10 Responses to a Step-Steer Manoeuvre on a Surface with Varying Friction**

## 5 CONCLUSIONS

In the present work a vehicle modelling approach is presented, which encompasses a number of essential elements for the simulation of severe handling manoeuvres. It is shown that, under critical conditions, the accurate modelling of the suspension is of paramount importance. Whereas commercial multi-body software packages offer capabilities and flexibility which is hard to challenge, simpler solutions might offer comparable accuracy and additional benefits, such as fewer parameters and reduced computational cost. This is demonstrated through extensive comparison of results generated by the proposed vehicle model with results obtained by the significantly more complex ADAMS model and by the real vehicle. The small differences observed in the results are primarily due to the lack of provision for steer and suspension compliance in the 14 DOF model. Also, secondary effects such as bump-steer were not included in the model. The inclusion of such effects can be seen as a potential future enhancement for the proposed model, likely to improve accuracy further. The analysis concludes with a virtual study of the propensity of the vehicle to roll. The concept of a road with uneven friction appears interesting, however it should always be expected that higher levels of friction promote higher lateral acceleration and therefore contribute towards roll-over. A more thorough study should involve a more detailed representation of the interaction between the tyres and potential obstacles. Finally, the proposed vehicle model is a primary candidate for the development of control strategies or for conducting iterative optimisation studies, areas where open model architecture and computational efficiency play an important role.

## ACKNOWLEDGMENTS

The authors wish to express their thanks to Professor J. Christian Gerdes for extending his support in brake system modelling.

# NOMENCLATURE

| | | |
|---|---|---|
| $\omega$ | - | Wheel angular velocity |
| $\delta$ | - | Steering road wheel angle |
| $\gamma$ | - | Camber angle |
| $\phi,\theta,\psi$ | - | Euler angles (roll, pitch, yaw) resulting from angular velocity transformation |
| $\Sigma F_x, \Sigma F_y, \Sigma F_z$ | - | Sum of forces in the direction of X,Y,Z of SAE frame of reference |
| $\Sigma M_x, \Sigma M_y, \Sigma M_z$ | - | Sum of moments about the X,Y,Z of SAE frame of reference |
| $\phi_{wheel}$ | - | Wheel roll angle because of uneven wheel vertical displacement |
| $jy_{contact}, jx_{contact}$ | - | Displacement of contact patch in x & y direction due to suspension geometry |
| $jz_{contact}$ | - | Displacement of contact patch in the vertical direction |
| B,C,D,E | - | Magic Formula tyre coefficients |
| $C_{f,r}$ | - | Suspension damping function |
| $C_{tyre}$ | - | Tyre damping coefficient |
| $F_{susp}$ | - | Suspension spring and damper force |
| $F_{tyre}$ | - | Tyre vertical spring and damper force |
| $F_{x,y\ tyre}$ | - | Tyre forces (Magic Formula) expressed in tyre SAE frame |
| $F_{zy}, F_{zx}$ | - | Suspension rigid reaction because of jacking / anti dive phenomena |
| $h_o$ | - | Origin of SAE frame of reference from ground |
| $I_{wheel}$ | - | Wheel Inertia |
| $I_{xx}, I_{yy}, I_{zz}$ | - | Sprung mass principal moments of inertia |
| $I_{xy}, I_{yz}, I_{zx}$ | - | Sprung mass product moments of inertia |
| $K_{f,r}$ | - | Suspension wheel rate function |
| $K_{roll}$ | - | Roll stiffness due to anti-roll bar |
| $K_{tyre}$ | - | Tyre stiffness coefficient |
| $m_s$ | - | Sprung vehicle mass |
| $m_T$ | - | Total mass of the vehicle |
| $M_{wheel}$ | - | Mass of the wheel assembly |
| p,q,r | - | Rotational velocities (roll, pitch, yaw) in the SAE frame of reference |
| $r_w$ | - | Tyre rolling radius |
| $T_B$ | - | Brake torque |
| Td | - | Driving torque |
| $t_{rf}, t_{rr}$ | - | Half track width at the front and rear |
| U, V, W | - | Translational velocity in the SAE frame of reference |
| X,Y,Z | - | Axes of the SAE frame of reference |
| $x_G, y_G, z_G$ | - | Position of the CG of the vehicle from the origin of SAE frame of reference |
| $z_{body}$ | - | Vehicle body displacement at four corners |
| $z_{wheel}$ | - | Wheel vertical displacement |

## REFERENCES


1. Pacejka, H.B., *Tyre and Vehicle Dynamics*. Oxford: Butterworth-Heinemann, 2002
2. Blundell, M.V., *The Modelling and Simulation of Vehicle Handling Part 1: Analysis Methods.* Proceedings of the I MECH E Part K Journal of Multi-body Dynamics. 213(no. 2): p. 103-118, 1999
3. Blundell, M.V., *The Modelling and Simulation of Vehicle Handling Part 2: Vehicle Modelling.* Proceedings of the I MECH E Part K Journal of Multi-body Dynamics. 213(no. 2): p. 119-134, 1999
4. Blundell, M.V., *The Modelling and Simulation of Vehicle Handling Part 3: Tyre Modelling.* Proceedings of the I MECH E Part K Journal of Multi-body Dynamics. 214(no. 2): p. 1-32, 2000
5. Blundell, M.V., *The Modelling and Simulation of Vehicle Handling Part 4: Handling Simulation.* Proceedings of the I MECH E Part K Journal of Multi-body Dynamics. 214(no. 2): p. 71-94, 2000
6. Hegazy, S., H. Rahnejat, and K. Hussain, *Multi-body dynamics in full-vehicle handling analysis under transient manoeuvre.* Vehicle System Dynamics. 34(1): p. 1-24, 2000
7. Shabana, A.A., *Dynamics of Multibody Systems*: Cambridge University Press, 2005
8. Rahnejat, H., *Multbody Dynamics - Vehicles, Machines and Mechanisms*: Professional Engineering Publishing Limited, 1998
9. Kortum, W. and R.S. Sharp, *Multibody Computer Codes in Vehicle System Dynamics*. Supplement to Vehicle System Dynamics, Volume 22: Swets & Zeitlinger, 1993
10. Ellis, J.R., *Vehicle Handling Dynamics*: London : Mechanical Engineering Publications, 1994
11. Satria, M., *Nonlinear Adaptive Filter Design for Integrated Vehicle Handling Dynamics State Estimation*, in *Aeronautical and Automotive Engineering*. Loughborough University: Loughborough, 2007
12. Renfroe, D., A. Roberts, and M. Gilbert, *Vehicle rollover maximum limits.* International Journal of Vehicle Design. 40(1-3): p. 144-158, 2006
13. Hac, A. *Rollover Stability Index Including Effects of Suspension Design*. in *SAE 2001 World Congress, SAE 2002-01-0965*. Detroit, MI, USA: SAE, Warrendale, PA, USA, 2002

14. Allen, R.W., et al., *Computer Simulation Analysis of Light Vehicle Lateral/Directional Dynamic Stability.* SAE Technical Paper Series, SAE 1999-01-0124, 1999
15. Meriam, J.L. and L.G. Kraige, *Engineering Mechanics Vol.1, Statics*. 3 ed. Vol. 1: John Wiley, 1993
16. Meriam, J.L. and L.G. Kraige, *Engineering Mechanics Vol.2, Dynamics*. 3 ed. Vol. 2: John Wiley, 1993
17. *Vehicle Dynamics Terminology, SAE J670e*, 1976
18. Cook, M.V., *Flight Dynamics Principles*: Butterworth Heinemann, 1997
19. Happian-Smith, J., *An Introduction to Modern Vehicle Design*: Butterworth-Heinemann, 2002
20. Gerrard, M.B., *Roll Centers and Jacking Forces in Independent Suspensions - A First Principles Explanation and a Designer's Toolkit.* SAE Technical Paper Series, SAE 1999-01-0046, 1999
21. Bakker, E., H.B. Pacejka, and L. Lidner, *A New Tire Model With An Application in Vehicle Dynamics Studies.* SAE Technical Paper Series, SAE 890087, 1989
22. Gerdes, J.C. and J.K. Hedrick, *Brake System Modeling for Simulation and Control.* Journal of Dynamic Systems, Measurement and Control, Transactions of the ASME. 121: p. 496-503, 1999
23. Fisher, D.K., *Brake System Component Dynamic Performance Measurement and Analysis.* SAE Technical Paper Series, SAE 700373, 1970
24. Khan, Y., P. Kulkarni, and K. Youcef-Toumi, *Modeling, experimentation and simulation of a brake apply system.* Journal of Dynamic Systems, Measurement and Control, Transactions of the ASME. 116(1): p. 111-119, 1994
25. BS ISO 3888-1, *Passenger cars –Test Track for a Severe Lane-Change Manoeuvre. Part 1: Double-Lane Change*. BRITISH STANDARD BS ISO 3888-1:1999, 1999